

X-ray spectroscopy of the supernova remnant RCW 86

A new challenge for modeling the emission from supernova remnants

Jacco Vink, Jelle S. Kaastra, and Johan A. M. Bleeker

Space Research Organization Netherlands, Sorbonnelaan 2 NL-3584 CA Utrecht, The Netherlands

Abstract. We present an analysis of ASCA X-ray data of SNR RCW 86. There appears to be a remarkable spectral variation over the remnant, indicating temperatures varying from 0.8 keV to > 3 keV. We have fitted these spectra with non-equilibrium ionization models and found that all regions are best fitted by emission from a hot plasma underabundant in metals (< 0.25 solar), but in some cases fluorescent emission indicates overabundances of Ar and Fe. The ionization stage of the metals appears to be far from equilibrium, at some spots as low as $\log(n_{\text{e}}t)$ (m^{-3}s) ~ 15.3 . We discuss the physical reality of the abundances and suggest an electron distribution with a supra-thermal tail to alleviate the strong depletion factors observed. We argue that RCW 86 is the result of a cavity explosion.

Key words: Atomic Processes; ISM: abundances – ISM: individual objects: RCW 86 – ISM: supernova remnants – X-rays: spectroscopy

1. Introduction

RCW 86 (also G315.4-2.3 and MSH 14-63) was for some time regarded as the historical remnant of the supernova (SN) of AD 185 (Clark & Stephenson 1977). Recently, however, Chin & Huang (1994) presented convincing evidence that the event recorded by the Chinese was not a SN at all. This makes RCW 86 just one of many other galactic supernova remnants (SNRs). Nevertheless, the ASCA X-ray spectra show that RCW 86 has some very special properties.

The radius of the remnant is $\sim 22'$. Distance estimates were usually based on the notion that RCW 86 was SN185. The most recent (kinematic) distance estimate is 2.8 kpc (Rosado et al. 1996).

Send offprint requests to: J.Vink@sron.ruu.nl

2. The data

Our analysis is mainly based on archival ASCA data (Tanaka et al. 1994). RCW 86 was observed by ASCA in the PV phase on August 17, 1993. Three pointings were used. Two of the pointings (together ~ 14 ks) cover the bright boomerang shaped area in the Southwest of the remnant. The third observation (~ 14 ks) covers the Northeastern part of the remnant. The Northwestern part of the remnant is not covered. The area covered by ASCA is indicated in the ROSAT PSPC image Fig. 1.

For our analysis we used spectra from all four instruments on board ASCA (i.e. SIS 0&1, GIS 2&3). The spectral resolution of the SIS instruments is better than that of the GIS (2% vs. 8% FWHM at 6 keV), but the latter have the advantage of better sensitivity at high energies. SIS observations were made in 4 CCD faint and bright modes.

We reduced the data with the NASA/HEASARC *ftools* package v3.6 using standard screening criteria. Background spectra were extracted from the standard background data available at the HEASARC archive. The response matrices for the SIS spectra were generated with *sirmg*, adding matrices of the various chips with the appropriate statistical weights and auxiliary response files.

The angular resolution of the ASCA instruments ensures that potential contamination by the galactic ridge is negligible (Claas et al. 1989, Kaastra et al. 1992).

We also analyzed archival ROSAT PSPC data of RCW 86. Three pointings focus on the North and one on the South of the remnant. The PSPC has the advantage of having a better spatial resolution (FWHM $\sim 30''$), than ASCA (FWHM $\sim 60''$), but the spectral resolution is poor. PSPC data were reduced with the *ftools* package as well.

3. Spectral analysis and interpretation

Spectral modeling. As a starting point for looking for spectral variation over the remnant we made hardness ratio maps for all pointings and instruments. Rather than showing all ASCA ratio maps, we present here the ROSAT

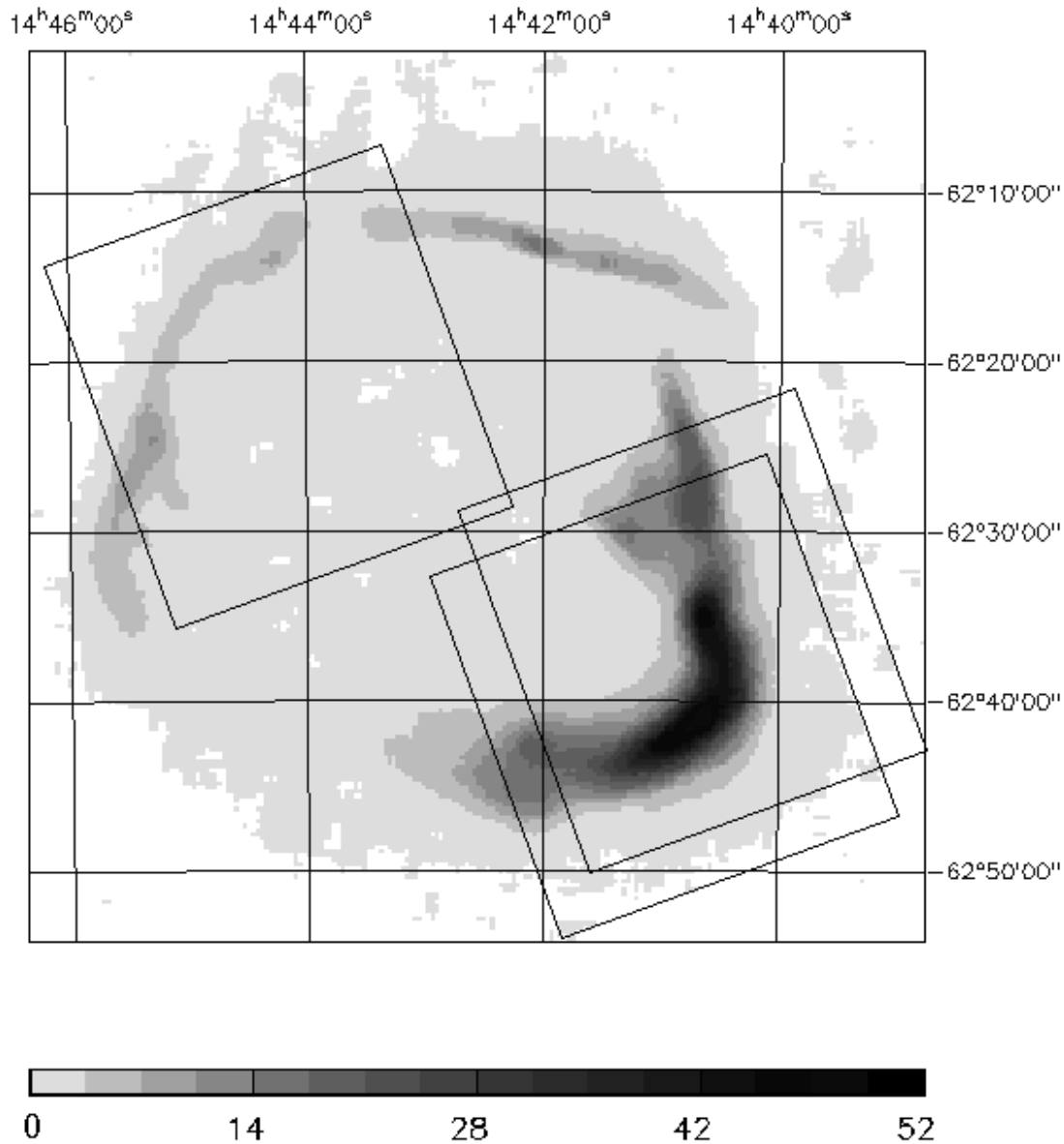


Fig. 1. The ROSAT PSPC image of RCW 86 in the energy range 0.1-1 keV. The image is composed of three observations, with a total integration time of 9ks. The image was smoothed with a median filter of 7×7 pixels, the pixel size being $15''$. The grey scale is such that one can see a clear distinction between the faint emission (the lightest grey) and the bright shell already known from the Einstein (Pisarski et al. 1984) and EXOSAT missions (Claas et al. 1989). Note that the satellite pointing was such that the Southwestern region was observed with less sensitivity than the Northeastern region. The three squares indicate the areas covered by the ASCA SIS instruments.

PSPC ratio map (Fig. 2¹). Note that with the spatial resolution of ASCA these regions were less distinct than in Fig. 2. So the spectral differences shown in Fig. 3 may in reality be larger. Because the ratio map does not give a good impression of the morphology of the remnant, we also present a PSPC image of RCW 86. Fig. 1 shows that the X-ray emission extends beyond the main shell. This was

¹ A color version and other images are available at <http://saturn.sron.ruu.nl/~jaccov/>

not seen in the HRI image by Pisarski et al. 1984. In particular the *Northwest* of the remnant shows faint emission outside the main shell. This cannot be an effect of the point spread function or interstellar scattering, because then one would expect a similar effect for the *Northeast* of the remnant, where the main shell is as bright as in the Northwest. Furthermore interstellar scattering takes place preferentially at lower energies (the photon cross section scales as E^{-2} , see Predehl & Schmitt 1995), whereas Fig. 2

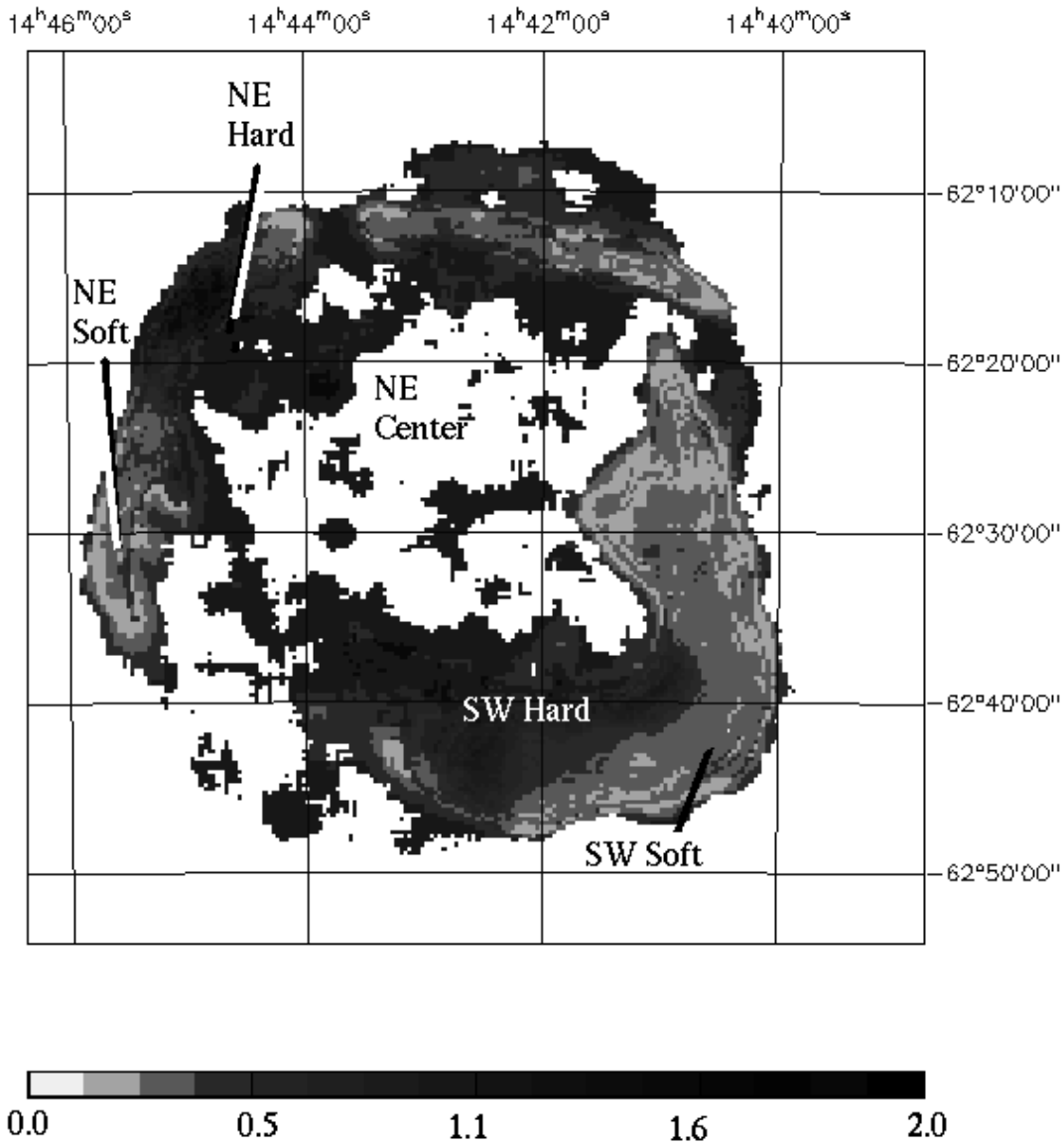


Fig. 2. The PSPC ratio map, based on the same observations as Fig. 1. The images are composed of three observations, with a total integration time of 9ks. The images were extracted in the energy ranges 0.1–1 keV and 1–2.1 keV and smoothed with a median filter of 7×7 pixels, the pixel size being $15''$. A higher ratio indicates a harder spectrum. The color scale is such that they represent our choice for selection of spectrum well.

shows that the faint emission in the Northwest is rather hard. Finally note that the $H\alpha$ image (Smith 1997) and the radio surface brightness profile (Pisarski et al. 1984) show also emission outside the main shell. For $H\alpha$ the emission seems to come from breakouts from the main shell.

The ratio map shows that we can identify two distinct regions in the Southwest (SW). For obvious reasons we will call spectra from these regions SW Hard and Soft. The SW Soft region correlates very well with the $H\alpha$ emission (Smith 1997), whereas the SW Hard region shows a rough correlation with the radio map (Kesteven & Caswell

1987). The SW Soft region is essentially the same as the bright boomerang-shaped shell in Fig. 1, although the SW Hard region has some overlap with this shell, suggesting a projection effect.

In the fainter Northeastern (NE) part of the remnant we also find hardness variations. The spectra of the hardest region we will tag NE Hard. We extracted spectra East of this, including the bright arm (NE Soft) and more to the center of the remnant (NE Center). As Fig. 3 shows the spectra are distinctively different, but all have a characteristic peak arising from helium-like Ne around 0.9 keV.

Table 1. Plasma parameters for one and two temperature fits to the ASCA spectra. The abundances are number abundances in fractions of solar abundances (Anders & Grevesse 1989). Numbers in brackets give the 90% confidence range ($\Delta\chi^2 = 2.7$).

	SW Soft		SW Hard		NE Soft		NE Center		NE Hard	
$n_e n_H V/d^2$ ($10^{62} \text{m}^{-3} \text{kpc}^{-2}$)	11		11		3		1.3		2.4	
kT_e (keV)	0.79	(0.73–0.85)	1.2	(1.0–1.4)	0.6	(0.5–0.9)	0.8	(0.6–1.1)	2.0	(1.8–2.1)
$n_e t$ ($10^{15} \text{m}^{-3} \text{s}$)	9.8	(9.0–11)	5.6	(5.0–6.1)	11	(7–20)	2.6	(< 8)	1.7	(1–3)
$n_e n_H V/d^2$ ($10^{62} \text{m}^{-3} \text{kpc}^{-2}$)	–		1.9		0.3		0.26		–	
kT_e (keV)	–		5	(> 3.7)	3.7	(2.2–9)	5	(> 3.7)	–	
$n_e t$ ($10^{15} \text{m}^{-3} \text{s}$)	–		0.7	(< 2.6)	2.5	(1–5)	3.5	(< 4.7)	–	
N	0	(0–0.04)	0	(0.0–0.01)	0.02	(0–0.2)	0.03	(0–0.3)	0	(0–0.03)
O	0.09	(0.06–0.12)	0.014	(0.008–0.021)	0.01	(0.02–0.1)	0.012	(0–0.06)	0	(0–0.002)
Ne	0.25	(0.21–0.28)	0.078	(0.065–0.086)	0.08	(0.10–0.25)	0.08	(0.04–0.5)	0.04	(0.03–0.05)
Mg	0.12	(0.10–0.15)	0.06	(0.04–0.07)	0.07	(0.04–0.14)	0.13	(0.03–0.5)	0.03	(0.0–0.09)
Si	0.19	(0.14–0.24)	0.15	(0.10–0.20)	0.15	(0.07–0.24)	0.16	(0–0.7)	0.3	(0.1–0.5)
S	0.3	(0.0–0.6)	0	(0–0.2)	0	(0–0.4)	0	(0–1.2)	0.12	(0.0–1.0)
Ar	8	(4.0–13)	0	(0–2.5)	10	(5–17)	0	(0–3)	0	(0.0–2.0)
Fe	0.16	(0.14–0.20)	0.12	(0.09–0.16)	0.10	(0.01–0.2)	0	(0–> 10)	2.8	(0.1–8)
Fe (hottest component)	–		2	(1–3)	6	(2–21)	2	(0–5)	–	
N_H (10^{21}cm^{-2})	2.3	(2.0–2.7)	1.6	(1.3–2.0)	2.7	(1.8–4.2)	2.0	(0.5–3.5)	1.3	(1.0–1.7)
χ^2_ν	4.7		1.7		1.2		1.8		1.7	

The NE spectra are in general harder than the SW spectra. The correlation between faintness and hardness (the softest emission comes from the brightest regions) suggests that the shock has decelerated in the densest region compared with the fainter regions such as the Northeast.

As noted above ASCA has a fairly large point spread function with broad wings making that the half power diameter is $3'$ (Tanaka et al., 1994, Serlemitsos et al. 1995). One might wonder how this affects the spectra in Fig. 3. Most serious is the contamination of the SW Hard spectrum by emission from the SW Soft region for energies around 1 keV. For higher energies (> 2 keV) it is the other way around. As an example, based on the PSPC image and spectra we estimate that the contribution of the emission from the soft region on the spectrum of the hard region is less than 25% at 1 keV. Such differences are much smaller than the overall differences between both spectra (Fig. 3).

We fitted the spectra from all regions with one and two temperature component NEI models using the spectral code SPEX (Kaastra et al. 1996). The free parameters were: the emission measure (EM) $n_e n_H V/d^2$ (where d is the distance, n_H and n_e , the hydrogen and electron number densities and V the volume occupied by the plasma); the ionization parameter $n_e t$ (t being the time since the plasma was heated); the electron temperature T_e ; the interstellar column density N_H and the abundances of N, O, Ne, Mg, Si, S, Ar and Fe. Since in some cases the Fe abundance can be estimated from both the Fe-L and Fe-K emission, we left the Fe abundance of the hot (i.e. Fe-K emission) and cool component free. In most cases the temperature of the hot component was not very well determined; in order to prevent temperatures much in excess of what was found by Ginga (Kaastra et al. 1991) we set an upper limit to the temperature of $kT_e = 5$ keV. We have used the interstellar extinction model of Morrison & McCammon (1983). Table 1 lists the results.

Abundances. There are two remarkable things to be noted about the best fitting models. First, the $n_e t$ values are very low, in some cases as low as $2 \cdot 10^{15} \text{m}^{-3} \text{s}$, one of the lowest value ever reported ($n_e t$ values a factor ten lower were recently reported for some regions of the Vela SNR based on ROSAT PSPC spectra, Bocchino et al., 1997). Second, the abundances are peculiar. In general, the abundances are low, except for some cases of Ar and Fe. The high Fe abundance is not simply an artefact of the model, which is clear from Fig. 4. It shows that the centroid of the Fe-K complex is at 6.4 keV, indicating a fluorescent origin. The Ar fluorescent emission at 3 keV is present in both the SIS (Fig. 3) and the GIS spectra. Note that fluorescence caused by irradiance is very unlikely in view of the large column densities and the large radiation field needed. So are the low abundances real? What could possibly be the origin of the abundance pattern? An approach to these problems is to analyze the assumptions made in fitting the spectra.

In the spectral code abundances are essentially determined by the line to continuum ratios. The continuum is supposed to be mainly bremsstrahlung from electron-ion collisions, assuming a Maxwellian electron energy distribution. Furthermore, the assumption is made that the plasma can be approximated by a simple one or two component plasma model assuming constant temperature, although in reality temperature and density gradients must be present. For most SNRs such a model works reasonably well. A possible extra source of continuum radiation can originate from synchrotron radiation arising from shock accelerated electrons with energies of the order of a few TeV. Such a model has been proposed for SN 1006 (Koyama et al. 1995). However, in our case this explanation does not work. First of all, the SW Soft spectrum is too soft to be dominated by a synchrotron component which is usually assumed to have a power law behaviour.

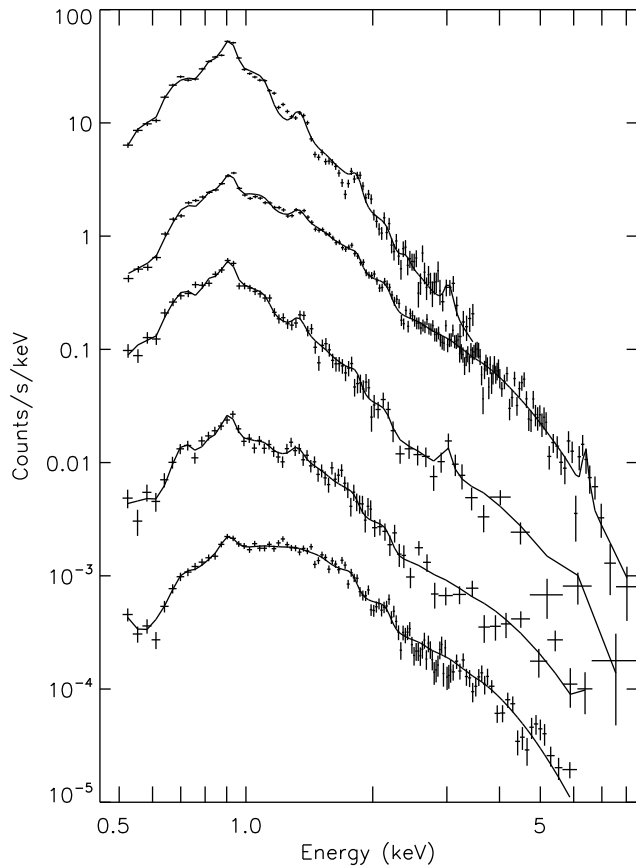


Fig. 3. SIS spectra of various regions together with NEI model spectra (solid lines). From top to bottom: SW Soft ($\times 10$), SW Hard, NE Soft, NE Center ($\times 0.1$), NE Hard ($\times 0.005$).

The second reason is even more compelling: a power law component makes it even harder to understand why we see such a relatively strong Fe-K complex around 6.4 keV.

Another way to deal with underabundances, dust depletion, is very unlikely in this case because the abundance pattern we find is not what one expects it to be in case of dust depletion. For instance Ne is underabundant, whereas it cannot be depleted in grains. Nevertheless, although it does not explain our overall results, dust depletion may give an additional effect for some metals (O, Mg, Si, Fe).

One might also think that an increased He/H ratio with respect to the solar value results in a stronger continuum emission and thus in a smaller line to continuum ratio. However, this is not the case. To see this, consider two plasmas, one with a solar He/H ratio and one for which part of the H has been used to make He (mostly ^4He). Because 4 H ions provide more electrons than one He ion, the plasma with the solar He/H ratio will emit more bremsstrahlung continuum.

So we probably need a modification of the standard model. A possibility is that the electron distribution is not Maxwellian. The continuum emission may partly result

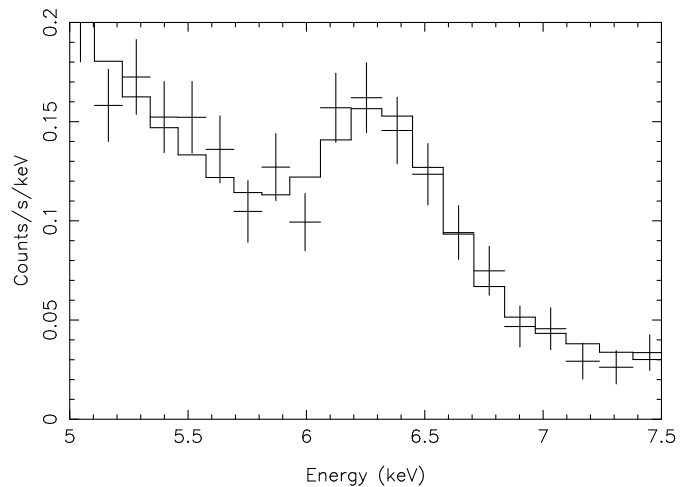


Fig. 4. The Fe-K complex in the South as observed by GIS2 and GIS3 (combined in one spectrum). The centroid of the complex is 6.3 ± 0.1 keV consistent with a fluorescent origin.

from a (non-thermal) tail to a relatively cool ($\lesssim 0.05$ keV) electron distribution. As a result, metals should be in a lower ionization stage than implied by the model fits. Such a model does at least qualitatively explain why fluorescent emission indicates different (i.e. high) abundances.

We have tried to model such a distribution by calculating the ionization stages of O for a mix of a high (~ 5 keV) and low temperature electron distribution (~ 0.02 keV). This crude model indicates that we can hide an appreciable amount (40%) of metals as long as $n_e t$ is low (e.g. $\lesssim 5 \cdot 10^{15} \text{ m}^{-3} \text{ s}$ for a cool to hot ratio of 4 to 1). Note that an appreciable amount of cool electrons is not unlikely in the light of recent UV observations of SN 1006 (Laming et al. 1996), which indicated $T_e/T_{\text{ion}} \lesssim 0.05$. As an indication: a shock velocity for RCW 86 of 700 km/s (Long & Blair 1990) without electron-ion equilibration gives $kT_e = 0.0005$ keV; Laming et al.'s result suggests $kT_e \lesssim 0.05$ keV. Clearly the effects of a non-Maxwellian electron distribution need further modeling. It is furthermore unclear why all the spectra of RCW 86 share so many characteristics, whereas they are taken from very different regions.

Up to now we did not address the issue how projection or contamination effects may be responsible for the unusual ASCA RCW 86 spectra. In our opinion it is very hard to explain the near absence of line emission solely by projection effects without invoking an unconventional interpretation. In a model that uses projection effects the observer should see a superposition of a spectrum with a “normal” line to continuum ratio and a spectrum with an almost complete absence of lines. So the difficulty of how to suppress line emission remains unaltered in such a model. In fact we cannot exclude that the ASCA SIS spectra are superpositions of two opposite cases, but we

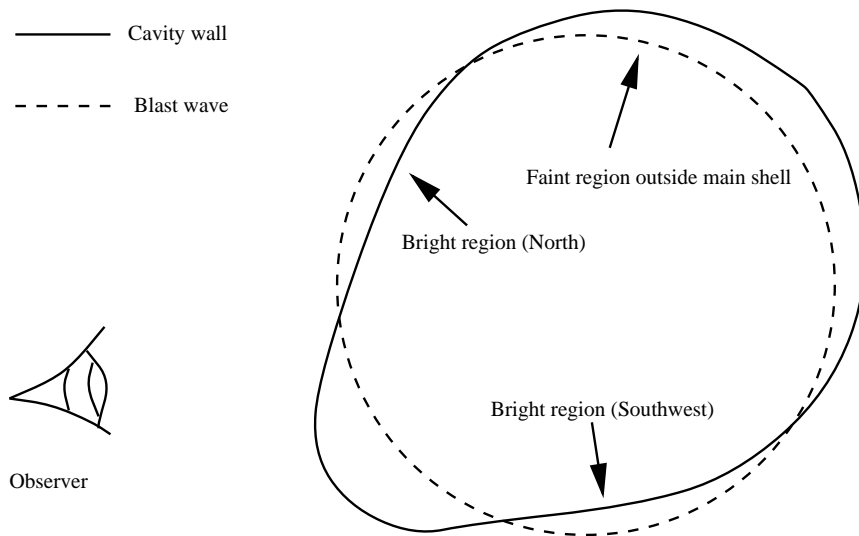


Fig. 5. A sketch of our interpretation of the structure of RCW 86 as a cavity explosion. We have drawn the blastwave here as a sphere, but in reality the shape of the blastwave will be affected when it hits the cavity wall. Bright are those regions where the blastwave has hit the cavity wall.

want to point out that it is remarkable that such extremely smooth spectra exist.

Evidence for a cavity explosion. Pisarski et al. 1984 and Claas et al. 1989 reported that there is a large density contrast between the North and South. In agreement with their results we find a (post shock) electron density of $(1 - 10) 10^6 d_{\text{kpc}}^{-0.5} \text{m}^{-3}$ for the SW Soft region and $0.2 10^6 d_{\text{kpc}}^{-0.5} \text{m}^{-3}$ for the NE region (d_{kpc} is the distance in kpc). The range in densities for the SW Soft region comes from the uncertainty in the emitting volume, which can be anything within a factor of 10 of $10^{50} d_{\text{kpc}}^3 \text{m}^3$. The estimate for the NE region was based on a filling factor of 0.25, a coverage by the Northeastern SIS pointing of 0.2 and a total EM of $5 10^{62} \text{m}^{-3} \text{kpc}^{-2}$. The optical emission tells an even more interesting story: $\text{H}\alpha$ observations of non-radiative shocks in the North give a pre-shock density of $0.2 10^6 \text{m}^{-3}$ (Long & Blair 1990), whereas spectra taken from the Southwest indicate densities of more than 10^8m^{-3} (Leibowitz & Danziger 1983).

The density contrast may have an accidental cause, but for a number of reasons we think that RCW 86 makes a strong case for being the result of a cavity explosion. In particular we think that the cavity wall has not been reached by the shock wave all over the remnant. With a cavity we mean here a tenuous region in the ISM blown by one or more stellar winds (Weaver et al., 1977), such a cavity is surrounded by a denser region, the cavity wall, consisting of swept-up material. The reasons for our hypothesis are: (1) the low density in the North, given the fact that RCW 86 is situated near the galactic plain; (2) the faint emission outside the main shell in Fig. 1, most notably in the Northwest, implying that the wall of the

cavity has not been reached in all directions (see Fig. 5); (3) Fig. 3 in Claas et al. (1989) shows that the radial X-ray profile of the Northeastern part of the remnant has too much emission coming from the shell of the SNR as compared to the Sedov model; (4) the more or less egg-shape reminds one of a cavity made by a star which was moving from North to South with respect to the interstellar medium (Weaver et al. 1977, see their Fig. 7), or alternatively the cavity may have been blown by several stars; (5) the gap in the Northern shell recalls the breakouts seen in numerical simulations of cavity SNRs by Franco et al. (1991). This is even more striking in the $\text{H}\alpha$ picture by Smith (1997) where ahead of the gap there is an enhancement in the $\text{H}\alpha$ emission; (6) a recent encounter of the blastwave with the cavity wall makes it more likely that complete electron heating has not yet occurred and may also explain why the $n_e t$ values are rather low: most of the matter has only recently been shocked when the blastwave hit the cavity wall.

In order to clarify point 2 we made a sketch of the structure of RCW 86 as we envision it (Fig. 5). Note that the figure gives a side view and that we do not know the inclination, so it might also be the Southwestern region that is closer to us. It is clear from our sketch that we do not know the exact shape of the cavity, because we only see those parts of the cavity wall that are lit up by the blastwave. However, it is also clear that if the cavity has an egg-like shape, the remnant will also have an egg-like shape, but possibly less elongated. Fig. 5 also clarifies the relatively low emission from the center of RCW 86 (point 3): along the line of sight the cavity wall has not yet been reached by the blastwave.

4. Conclusions

We have presented an analysis of ASCA spectra of RCW 86, which we modeled by NEI models. In general these models fit the data rather well, but indicate an underabundance of metals. On the other hand, we need overabundances to explain the fluorescent emission of Ar and Fe in some parts of the remnant. The fitted models indicate a very low $n_e t$ value.

We suggest that the peculiarities of the spectra may be the result of a non-Maxwellian electron distribution. If the bulk of the electrons has a very low temperature, most of the ions should be in a low ionization stage (e.g. the Li-like stage), whereas a supra-thermal tail may dominate the X-ray continuum and explain the Ar-K and Fe-K fluorescent emission. Note that our density calculations underestimate the true densities if the electron distribution is non-thermal.

Other SNRs may exhibit similar effects, although perhaps to a lesser extent. In that respect it is interesting that Miyata et al. (1994) and Miyata (1996) report similar underabundances for the Cygnus Loop.

We suggest that RCW 86 is the result of a cavity explosion. The morphology of the remnant is a good indication for that and even suggests that the cavity may have been blown by more than one star. This is interesting in view of the new distance estimate by Rosado et al. (1996), placing RCW 86 at the distance of an OB association at 2.5 kpc (Westerlund 1969). If the association is real, RCW 86 is probably the result of a SN type II explosion.

Acknowledgements. It is a pleasure to thank Dr. Y. Tanaka for fruitful discussions and his useful suggestions. We also thank the referee Dr. R. Strom for his critical reading of the article. This research has made use of data obtained through the High Energy Astrophysics Science Archive Research Center Online Service, provided by the NASA/Goddard Space Flight Center. This work was financially supported by NWO, the Netherlands Organization for Scientific Research.

References

- Anders, E., Grevesse, N., 1989, *Geochimica et Cosmochimica Acta* 53, 197
- Bocchino, F., Maggio, A., Sciortino, S., 1997, *ApJ* 481, 872
- Chin, Y.-N., Huang Y.-L., 1994, *Nat* 371, 398
- Claas, J.J., Smith, A., Kaastra, J.S., et al., 1989, *ApJ* 337, 399
- Clark, D.H., Stephenson, F. R., 1977, *The Historical Supernovae*, Pergamon Press, Oxford
- Franco, J., Tenorio-Tagle, G., Bodenheimer, P., Różycka, M., 1991, *PASP* 103, 803
- Kaastra, J.S., Asaoka, I., Koyama, K., et al., 1992, *A&A* 264, 654
- Kaastra, J.S., Mewe, R., Nieuwenhuijzen, H., 1996, In: Watanabe, T. (ed.) *The 11th coll. on UV and X-ray Spectr. of Astroph. and Laboratory Plasmas*, p. 411
- Kesteven, M.J., Caswell, J.L., 1987, *A&A* 183, 118
- Koyama, K., Petre, R., Gotthelf, E., et al., 1995, *Nat* 378, 255
- Laming, J.M., Raymond, J.C., McLaughlin, B.M., Blair, W.P., 1996, *ApJ* 472, 267
- Leibowitz, E.M., Danziger, I.J., 1983, *MNRAS* 204, 273
- Long, K.S., Blair, W.P., 1990, *ApJ* 358, L13
- Miyata, E., Tsunemi, H., Pisarski, R., et al., 1994, *PASJ* 46, L101
- Miyata, E. 1996, PhD thesis University of Osaka
- Morrison, R., McCammon, D., 1983, *ApJ* 270, 119
- Pisarski, R.L., Helfand, D.J., Kahn, S.M., 1984, *ApJ* 277, 710
- Predehl, P., Schmitt, J.H.M.M., 1995, *A&A* 293, 889
- Rosado, M., Ambrocio-Cruz, P., Le Coarer, E., et al., 1996, *A&A* 315, 243
- Serlemitsos, P.J., Jalota, L., Soong, Y., et al., 1995, *PASJ* 47, 105
- Smith, R.C., 1997, in preparation
- Tanaka, Y., Inoue, H., Holt, S.S., 1994, *PASJ* 46, L37
- Weaver, R., McCray, R., Castor J. et al., 1977, *ApJ* 218, 377
- Westerlund, B., 1969, *AJ* 74, 879